



Submarine hydrodynamics for off-design conditions

Serge Toxopeus¹ · Maarten Kerkvliet¹ · Roderik Vogels¹ · Frans Quadvlieg¹ · Bart Nienhuis²

Received: 29 April 2022 / Accepted: 17 August 2022 / Published online: 28 September 2022
© The Author(s) 2022

Abstract

Traditionally, submarine hydrodynamic design has focussed mainly on requirements regarding operational range, powering performance and manoeuvring ability for deeply submerged conditions. To improve the effectiveness of the boat, attention is also paid to operating near or at the surface and fortunately, computational tools and experimental methods are available to analyse the performance of submarines at these conditions. To advance submarine hydrodynamics knowledge and tools, DMO and MARIN have conducted a wide variety of bi-lateral or collaborative studies using potential and viscous flow methods and experiments on several submarine hull forms. In this article, several examples are presented of the development and use of hydrodynamic tools available during the design and assessment process of future submarines. These examples range from experimental and numerical studies into at-surface and periscope-depth resistance and powering, periscope-depth manoeuvring, high-fidelity flow around the boat during straight flight and manoeuvring motions, wakes of surface-piercing masts, to depth keeping under waves. It is demonstrated how state-of-the-art studies help in advancing the knowledge on submarine hydrodynamics and improving the overall design of modern submarines.

Keywords Submarines · Hydrodynamics · Off-design · ReFRESKO · Experiments · CFD · BB1 · BB2

Abbreviations

AMR	automatic mesh refinement	IDDES	improved delayed detached eddy simulation
AVT	applied vehicle technology	ISTAR	intelligence, surveillance, target acquisition and reconnaissance
BB1/2	Brendon's boat 1/2	LES	large eddy simulation
CFD	computational fluid dynamics	MARIN	maritime research institute Netherlands
CPMC	computerised planar motion carriage	NATO	North Atlantic treaty organisation
DMO	defence materiel organisation	PIV	particle image velocimetry
DSTG	defence science and technology group	RANS	Reynolds-averaged Navier–Stokes
		RSM	Reynolds stress model
		SOF	special operations forces
		SRS	scale-resolving simulations
		X-LES	extra-large eddy simulation

Maarten Kerkvliet, Roderik Vogels, Frans Quadvlieg and Bart Nienhuis contributed equally to this work.

✉ Serge Toxopeus
s.l.toxopeus@marin.nl

Maarten Kerkvliet
m.kerkvliet@marin.nl

Roderik Vogels
r.vogels@marin.nl

Frans Quadvlieg
f.quadvlieg@marin.nl

Bart Nienhuis
b.nienhuis@mindef.nl

¹ Maritime Research Institute Netherlands (MARIN), Wageningen, The Netherlands

² Defence Materiel Organisation (DMO), Utrecht, The Netherlands

1 Introduction

Traditionally, submarine hydrodynamic design has focussed mainly on requirements regarding operational range, powering performance and manoeuvring ability for deeply submerged conditions (van Terwisga and Hooft 1988). However, due to mission requirements and operational profiles, the boat should also perform well in service conditions. To improve the effectiveness of the boat, attention therefore needs also to be paid to for instance operating near or at the surface. For

tunately, computational tools and experimental methods are available to analyse the performance of submarines at these conditions (Overpelt 2014; Renilson 2018). These tools can also be used to better understand the impact of design details on the performance. With the progress of numerical capabilities, both in computational performance as in reliability and accuracy, computational fluid dynamics (CFD, meaning the computation of viscous flows) is more and more becoming the primary design tool of submarines.

To advance submarine hydrodynamic knowledge and tools and to support upkeep or successor programmes, DMO and MARIN have conducted a wide variety of bi-lateral or collaborative studies using empirical tools, potential and viscous flow methods and experiments on generic submarine hulls such as the SUBOFF (Toxopeus 2008; Vaz et al. 2010; Toxopeus et al. 2012), Joubert/BB1 (Joubert 2006; Kerkvliet 2013; Toxopeus et al. 2014; Overpelt 2014) and BB2 (Overpelt et al. 2015; Carrica et al. 2016; Toxopeus et al. 2019), but also on the existing Walrus class submarines (Bettle et al. 2010). These studies have led to increased applicability and accuracy of the submarine hydrodynamics toolkit.

In this article, several examples will be shown of the development and use of hydrodynamic tools available during the design and assessment process of future submarines. These examples range from experimental and numerical studies into at-surface and periscope-depth resistance and powering, periscope-depth manoeuvring, high-fidelity flow around the boat during straight flight and manoeuvring motions, wakes of surface-piercing masts, to depth keeping under waves. Prior to discussing the examples, the coordinate system used to show results will shortly be presented.

The experimental studies comprise captive (for instance CPMC) and free running model tests, while the numerical studies involve empirical tools, potential flow and viscous flow solvers.

The article will demonstrate how state-of-the-art studies help in advancing the knowledge on submarine hydrodynamics and improve the overall design of modern submarines.

2 Coordinate system

All results in this article are presented in a coordinate system usually adopted for manoeuvring studies, see Fig. 1. The origin of this right-handed coordinate system is located at the intersection of the longitudinal axis of symmetry of the hull, midship and centre-plane, with x directed forward, y to starboard and z vertically downward. All integral forces X , Y , Z and moments K , M , N are directed as shown in Fig. 1 and made non-dimensional with the overall length L of the

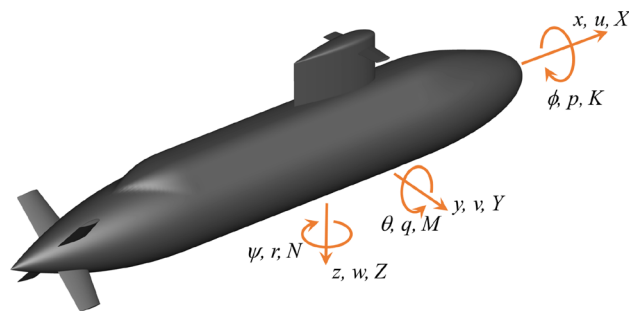


Fig. 1 Coordinate system

submarine using

$$X', Y', Z' = \frac{X, Y, Z}{\frac{1}{2}\rho V^2 L^2} \quad K', M', N' = \frac{K, M, N}{\frac{1}{2}\rho V^2 L^3},$$

where ρ is density, and V is the velocity of the submarine. The drift angle is defined by $\beta = \arctan \frac{-v}{u}$, with u and v directed according to the x - and y -axes of Fig. 1, respectively, which means β is positive for flow coming from port side. The angle of attack is defined by $\alpha = \arctan \frac{w}{u}$, which means α is positive for flow coming from below.

3 Experimental and numerical studies into at-surface resistance and powering

In the early design stage of a submarine, the need exists to determine the required propulsive power and to estimate the operational range of the submarine. These properties can be derived with high fidelity using model testing or CFD calculations. These do, however, require detailed knowledge of the submarine's design which is typically not known at this early stage. SUBMAR is an empirical tool developed by MARIN to predict the resistance and powering requirements of a submarine (van Terwisga and Hooft 1988). By only requiring main dimensions as input, SUBMAR can be used to explore various design choices in the early design stage.

SUBMAR is based on empirical relations and is capable of predicting resistance and propulsive power for deeply submerged, periscope depth and surfaced sailing conditions. The latter condition is of importance, as expeditionary diesel-electric type submarines sometimes sail in surfaced condition during (part of) their transit to the area of operations. When sailing in or close to the surface, the wave making resistance is the major component of the total resistance of the submarine.

In recent years, SUBMAR was improved to better predict the important wave making resistance when sailing at periscope depth and at the surface. Use was made of resistance and powering data at MARIN of eight different submarine designs. The data were obtained using CFD cal-

culations, potential flow calculations, model testing and from full scale trials. Two particularly interesting studies are highlighted in the following paragraphs.

3.1 Effect of L/D

From a resistance viewpoint for deeply submerged submarines there is an optimum length-to-diameter (L/D) ratio which gives the best compromise between friction and form drag (Renilson 2018). However, due to design and construction requirements, it is often easier for a given submarine displacement to have a relatively longer submarine with a reduced diameter compared to the optimum L/D . As such, it is important to be able to study the impact of L/D on the submarine resistance. The influence of L/D on the submerged resistance has been studied extensively in the past, see Gertler (1950), but the effect on the surfaced resistance also needs to be considered. To improve and validate SUBMAR for various L/D ratios, model tests have been performed where the L/D ratio of the BB2 submarine was varied from the original 7.3 to 12. Figure 2 shows these four variants being tested at the same speed and same draught (but free to trim and sink) in MARIN's deep water towing tank.

Based on these model tests where the L/D ratio was varied by increasing the length of the parallel midbody, it is concluded that the resistance increase due to an increased length of the submarine consists mainly of frictional resistance: increasing the length does not increase the wave making resistance. Furthermore, increasing the length increases the wake fraction w , while the thrust deduction fraction t is not affected. This means that increasing the L/D ratio, without changing the displacement, results in an improved hull

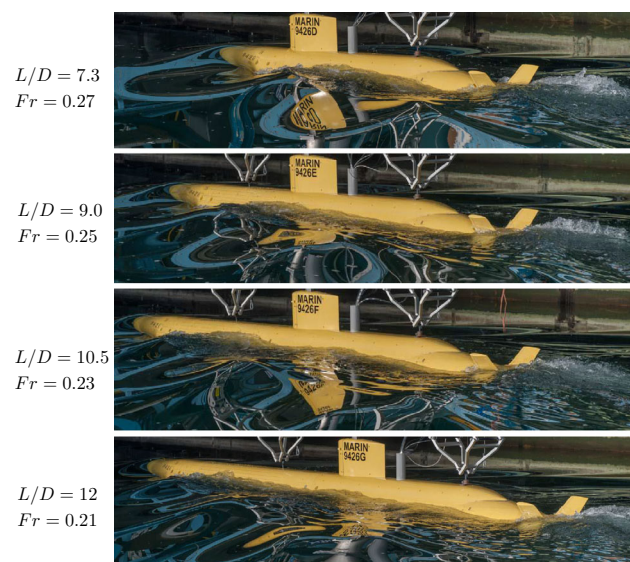


Fig. 2 Wave profiles at a speed corresponding to 14 kn on full scale of variants of the BB2 submarine at four L/D -ratios

efficiency $\eta_H = (1 - t)/(1 - w)$ and therefore improved propulsive performance. Hence, a large L/D ratio is preferred for surfaced sailing conditions.

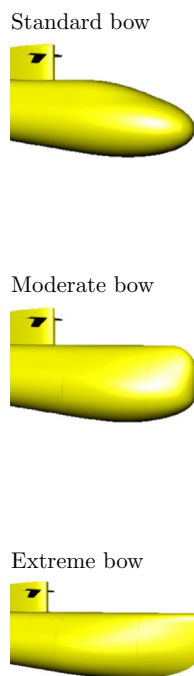
It should be noted that the different L/D ratios of the model during the experiments were realised by adding parallel midship sections to the model. This means that effectively the L/D ratio as well as the displacement ∇ of the model changed when the draught was kept constant. Furthermore, the tests at the same speed for the various length ratios imply different Froude numbers between variants. This approach provides the desired data for improving the SUBMAR predictions for surfaced conditions, while still being cost-effective considering model manufacturing costs. However, in normal design variations it would be desirable to maintain a constant displacement when increasing the L/D ratio, effectively reducing the diameter of the boat, and leading to slightly different Froude numbers than encountered during the model tests. Due to its generic nature and use of non-dimensional empiric formulae, SUBMAR is able to handle these design changes during predictions.

3.2 Effect of bow shape

Submarine bow shapes are typically optimised for deeply submerged sailing conditions. When sailing at the surface, this bow shape results in a significant wave making resistance. By changing the bow shape it is possible to reduce the bow wave and thus the wave making resistance.

To study the effect of the bow shape on both the surfaced and submerged resistance a series of resistance tests using the BB1 submarine hull form with three different bow shapes has been performed (Overpelt 2014) and the findings were incorporated in SUBMAR. Additionally, validation studies of REFRESCO (Vaz et al. 2009) predictions for surfaced resistance were done. REFRESCO is a CFD solver developed by MARIN based on a finite volume discretisation of the continuity and momentum equations written in strong conservation form. The free surface is captured with a Volume-of-Fluid interface capturing scheme (Klajj et al. 2018). The code has been widely applied to submarines and compared to experimental results or other solver results previously, see, e.g. Toxopeus et al. (2012), NATO AVT-301 (2022). Results of calculations with the SST turbulence model and Volume-of-Fluid interface capturing, with the boat free to sink and trim, show that the bow shape has a significant effect on the wave making resistance when sailing at the surface. A comparison of the bow wave, which is indicative of the wave making resistance, at the same sailing speed for the tested bow shapes is shown in Fig. 3. Overall, it is concluded that below about 7 kn, the wave resistance is nearly identical between the bow designs. Above 7 kn, up to the maximum tested speed, the alternative bow shapes have a resistance benefit. The extreme bow shape has a resistance

Fig. 3 Wave profiles at a speed corresponding to 12 kn on full scale of variants of the BB1 submarine with three different bow shapes of increasing fineness



reduction of 44% as compared to the standard bow when sailing at the surface at 12 kn ($Fr = 0.235$), whilst only showing an increase of 3% in the resistance when sailing deeply submerged. Also previous work by Power (1977) showed that changing the bow shape has relatively little effect on the submerged resistance of bodies of revolution. Of course, careful studies need to be included to ensure the performance of sensor and weapon systems placed in or near the bow which can be affected by the changes in bow shape.

It was also found that the dynamic trim and sinkage for surfaced conditions was influenced by the bow shape. The original bow had a more pronounced tendency to sink and trim by the bow during forward speed, such that there was an increased risk of propeller ventilation compared to the moderate and extreme bow shapes.

4 Periscope-depth operation in calm water

The analysis of a submarine travelling near the free surface is of interest since many manoeuvres require the submarine to be near the surface to accomplish a given task. Examples of these manoeuvres include snorting, but also ISTAR (Intelligence, Surveillance, Target Acquisition and Reconnaissance) and SOF (Special Operations Forces) operations in hostile waters. Many of these operations are performed while the submarine is in motion, which is why the understanding of the

hydrodynamic forces and moments are important to ensure all manoeuvres can be performed safely. As a result, various studies have been conducted at MARIN on submarines travelling near the free surface, both experimental and numerical, see, for example, Carrica et al. (2016). Another interesting study into exhaust gas plumes during snorting was done by Klapwijk et al. (2017).

One of the aspects of interest at periscope depth is the wave making resistance. Although fully submerged, a submarine sailing at speed at periscope depth will still generate waves and thus experience wave making resistance. This can efficiently be studied using potential flow calculations. An extensive series of calculations has been performed using MARIN's panel code RAPID (Raven 1996) for the BB2 hull form. Sailing depth and sailing speed were varied and the obtained wave profiles (an example is given in Fig. 4) and wave making resistances for each combination of speed and depth were incorporated in SUBMAR, such that it is possible to study the performance of a submarine in deeply submerged, periscope depth or surfaced conditions. The waves generated by the submarine can show a favourable interference, which is dependent on the sailing speed. The RAPID results clearly show which speeds are favourable from a resistance point of view, thus giving the operator important information on how to operate the submarine best.

When the tip of the sail is close to the surface, or during manoeuvring conditions, viscous effects such as flow

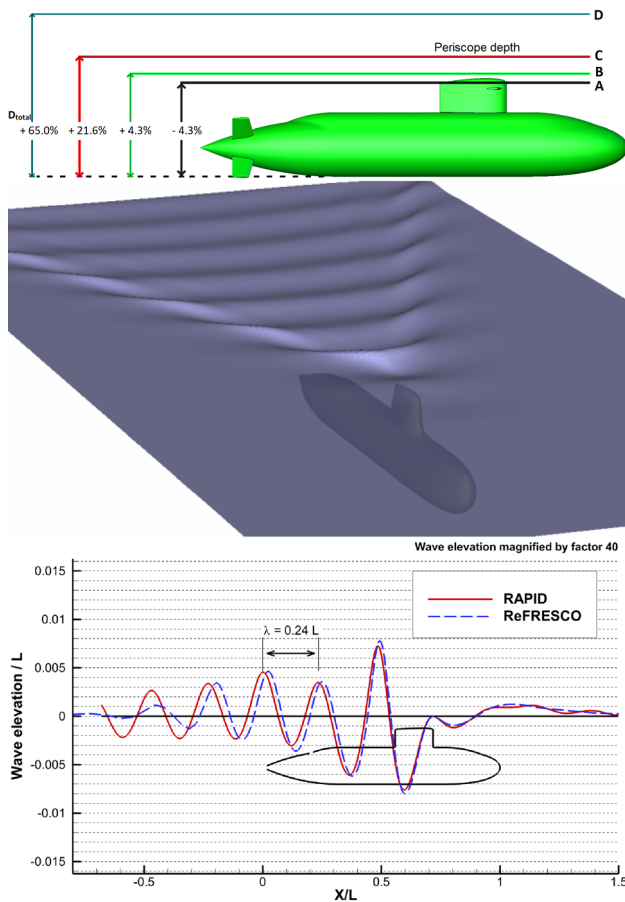


Fig. 4 Overview of submergence depths studied, with $D_{total} = 0.231 L = 1.69B$ the depth of the boat from keel to top of sail (top figure), RAPID wave system for a BB2 submarine variant sailing at periscope depth (middle) and wave elevation at centreline from RAPID and REFRESCO computations, $Fr = 0.196$, depth C (bottom)

separation or wave breaking become important which cannot reliably be captured by potential flow. Therefore, a need exists for viscous flow computations as well. Viscous flow simulations were performed with ReFRESCO for the fully appended BB2 submarine sailing near the free surface for sailing straight, steady drift and yaw rotation, see Torunski (2018). The straight sailing conditions were performed for four depth conditions, indicated by A, B, C and D, see Fig. 4 and some of the results are summarised here. The main objective was to gain knowledge on the effect of the free surface on the forces and moments acting on the submarine. The results of the REFRESCO viscous flow computations compared well to RAPID potential flow computations, as shown in Fig. 4, and the wave length λ matches the wave theory for deep water $\lambda/L = 2\pi Fr^2$. The decrease in wave amplitude behind the submarine in the REFRESCO simulations is due to lack of spatial grid resolution in that wake region.

The non-dimensional resistance and vertical forces (X' , Z') and pitch moment (M') are displayed in Fig. 5. There is a

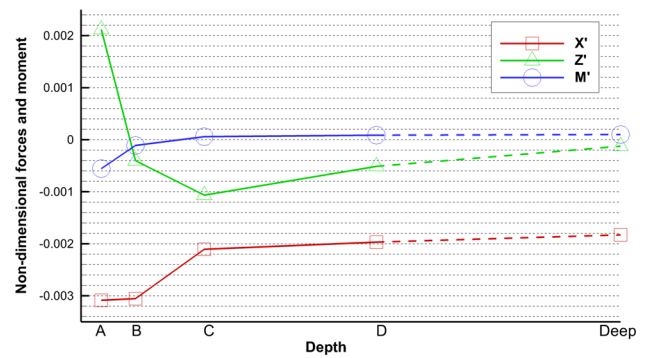


Fig. 5 Total forces and moments acting on the submarine at straight sailing conditions

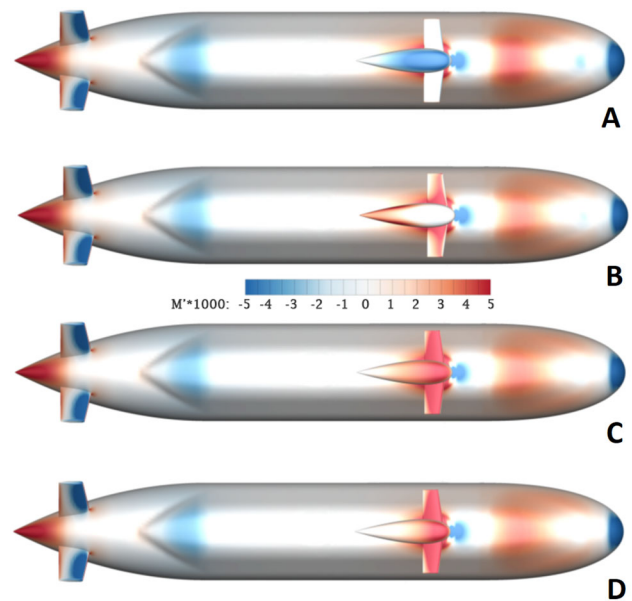


Fig. 6 Contribution to the pitch moment for each submergence depth (red indicates an area which contributes to bow-up and blue vice-versa)

significant change in the vertical forces acting on the submarine from the conditions C to A. This is due to the interaction of the free surface with the top of the sail and the sailplanes, as can be seen in Fig. 6. The iso-contours indicate whether an area contributes to a bow-up (red) or bow-down (blue) pitching moment. The out-of-plane force on top of the sail and the lifting forces from the sailplanes are different since a part of the sail is piercing the water surface in condition A and B. As a result the pitch moment changes sign.

More information regarding manoeuvring at periscope depth can be found in Torunski (2018).

5 High-fidelity flow field predictions

CFD can be used to predict the forces and moments acting on a submarine, but also to study in detail the flow around

design details. For example, so-called horse shoe vortices occur when a boundary layer developing on one surface is intersected by another surface, for instance near the roots of rudders, sailplanes or the sail. The horse shoe vortex developing at the junction of the casing and sail has been studied by, e.g. (Devenport et al. 1992). This horse shoe vortex is caused by interaction of the stagnation region at the leading edge of the sail with the boundary layer on the casing, leading to a flow circulation in the corner of the junction. The vortex wraps around the sail and progresses into the propeller plane, possibly causing fluctuations in the loads on the propeller, influencing the propeller performance and noise. CFD provides an opportunity to study the development of the horse shoe vortex and the influence of design changes on the propeller wake. For the BB1 hull form, such a study was conducted by Toxopeus et al. (2014), showing that applying a fillet or cuff in the sail-deck junction area and proper shaping of the sail tip could lead to a reduction of the resistance of several percent and a significant improvement of the propeller wake field. It was observed that the fillet effectively weakened the vorticity in the horse shoe vortex. The followed approach can also be used to design fillets for the control planes. Similar studies have been conducted to improve fairings around hull openings or protruding design details such as intercept sonars.

CFD can also be used to better understand features seen in the relation between angle of attack and the forces acting on the fully appended boat. For the BB2, for example, it can be found that at -12° of angle of attack α , a change of slope in the vertical force and pitch moment curves is present, see Fig. 7. Further inspection of the flow field highlights that at this specific angle, the tip vortices coming from the sailplanes interact with the upper rudders and subsequently change the trend in the loads on these rudders, see Fig. 8. This phenomenon is especially visible in the pitch moment, due to the large distance of the aft rudders to the centre of reference. This interaction between the sailplane tip vortices and the upper rudders can occur when pitching bow down during diving towards a larger depth and can lead to unexpected behaviour of the submarine during such manoeuvres.

Within the NATO AVT-301 Research Task Group, extensive comparisons between CFD predictions for the BB2 for captive manoeuvres are made (Toxopeus et al. 2019; NATO AVT-301 2022) to assess the state-of-the-art of CFD predictions for underwater vehicles. Each member of the group has made predictions for the BB2 at straight flight, 10° drift angle, or steady rotational motion with varying drift angles. The forces and moments acting on the boat and the flow around it have been carefully studied. Since validation data are only available from model experiments, all computations were done for model scale conditions, with Reynolds numbers ranging from $Re = 3.9 \times 10^6$ to 9.6×10^6 . From this extensive work, important conclusions can be drawn.

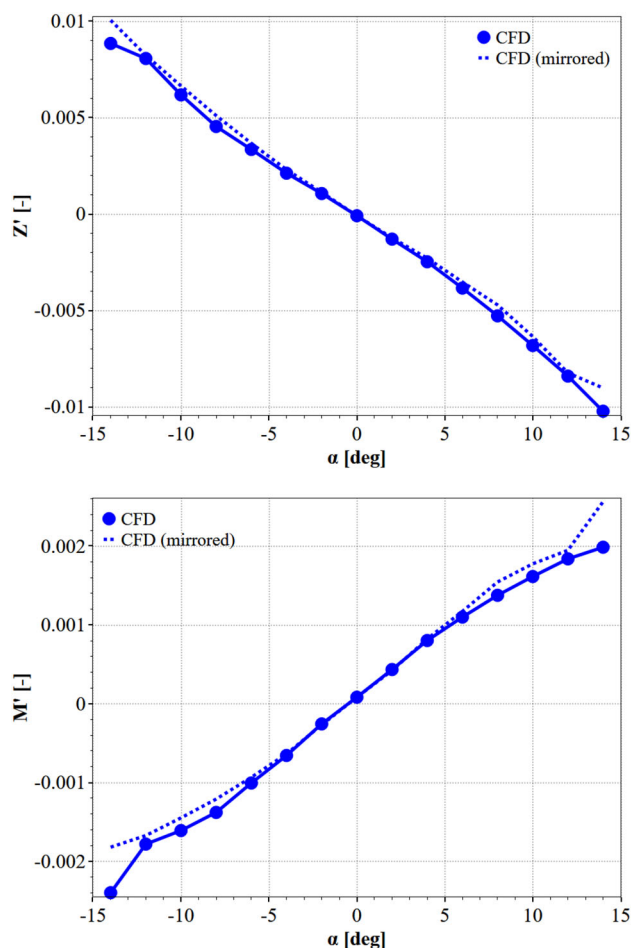


Fig. 7 Relation between angle of attack and vertical force (top) and pitch moment (bottom) on BB2

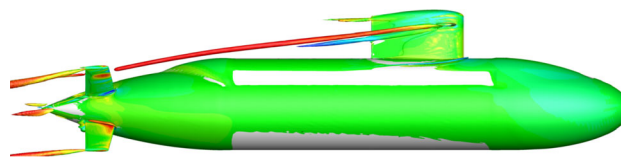


Fig. 8 BB2 at -12° angle of attack, visualisation of vortices

Regarding the forces and moments on the boat, discretisation errors can be identified when the grid is too coarse. In grids of 14M cells as used in the current study, a discretisation error of 5% was still present. For the flow field itself, and especially near the stern region, it was found that the most efficient results (from computational requirements perspective) with small discretisation errors were obtained with automatic mesh refinement (AMR) or dedicated refinement zones, leading to grids in the order of 100M cells or above. The application of AMR should, therefore, become standard practice in CFD. New cells added on the submarine surface can lead to jumps in the distribution of face normals and subsequently in irregular shear stress distributions. There-

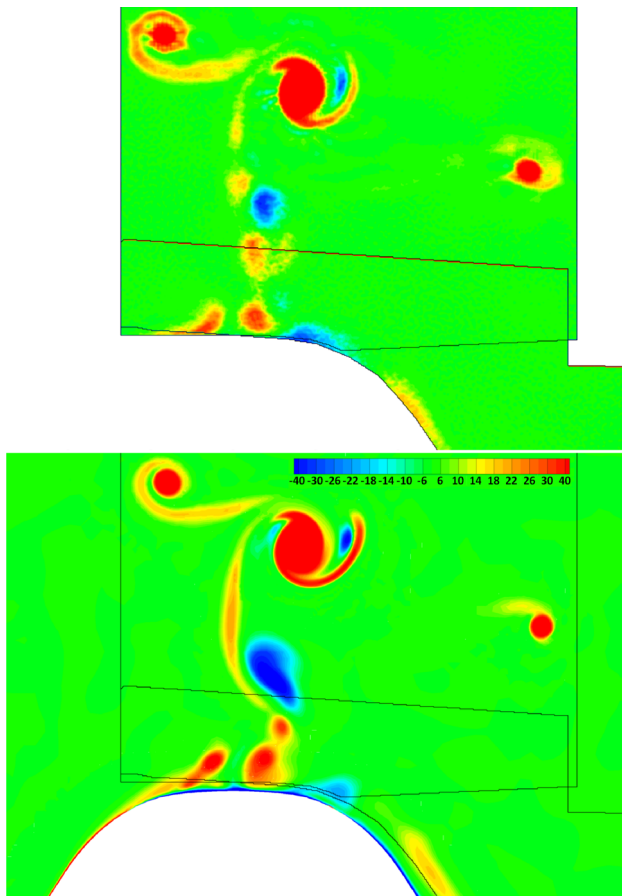


Fig. 9 Non-dimensional axial vorticity field behind the sail, $Re = 3.9 \times 10^6$, $\beta = 10^\circ$, DSTG experiment (top) vs. REFRESCO RSM+AMR (bottom)

fore, projection of these new cell faces onto the underlying geometry is required.

Based on comparisons with wind tunnel tests provided by DSTG (Lee et al. 2018) (test section of 6.55 m length, 2.74 m width and 2.13 m height), it is concluded that also the choice of turbulence model is important. For example, changing the turbulence model can result in a change of predicted resistance of up to 10%. Additionally, the turbulence model choice influences the prediction of details in the flow field. The MARIN predictions that showed the best agreement with the experiments for the 10° drift angle were obtained using the RSM SSG/LRR turbulence model (Eisfeld and Brodersen 2005), see Fig. 9. More validation of RSM predictions is recommended to assess the performance of this turbulence model for submarine hydrodynamics.

QinetiQ performed rotating arm experiments for the BB2. CFD simulations for these conditions showed comparison errors in the computations. Differences in the CFD results were observed due to the choice of turbulence model and grid density, but also due to numerical setup details and the CFD solver. The predicted forces and moments acting on the hull of the submarine showed good agreement between

the submissions, but the loads on especially the aft control surfaces are highly dependent on whether rudder stall is predicted or not by a given submission. This clearly indicates that, due to the high incidence angles occurring at the aft rudders, the prediction of rotational motion with CFD is still not fully under control and needs more attention.

Preliminary predictions using scale-resolving simulations (for example IDDES or LES) either led to incorrect predictions of the frictional resistance due to relaminarisation of the flow in the computations, or did not lead to improvements compared to conventional RANS predictions. Overall, it was found that to improve CFD predictions, more attention to the estimation of the uncertainties in the experiments is required.

Recently, DMO has performed measurements in the DNW-NWB aeroacoustic wind tunnel (test section of 3.25 m length, 2.8 m width and 6 m height), using high-speed and high-resolution two-dimensional three-component Particle Image Velocimetry (2D-3C PIV) and hotwire anemometry to capture the detailed flow, and pressure probes and microphone arrays to obtain pressure fluctuations and flow and propeller noise. These results will be used in future work for validation of scale-resolving CFD predictions.

6 Wakes of surface-piercing masts

Not only the wave pattern generated by the boat and sail can contribute to increased visibility or resistance during operations at periscope depth, but also masts protruding the water surface, such as a periscope for example. Therefore, an experimental and numerical study into the wave patterns behind a surface piercing mast has been conducted. Inspired by Hay (1947), tests were performed at MARIN at multiple speeds with a schematic surface piercing truncated cylinder with a realistic full scale diameter, clamped at the top to the towing carriage and the tip extending sufficiently far below the water surface to avoid end effects, see Fig. 10. During the experiments, the wave elevations behind and next to the mast and the loads acting on the mast were measured, while also the wave pattern was recorded using several video cameras. For selected test conditions, also REFRESCO computations were carried out.

The experimental results at one of the wave probes along the basin are displayed in Fig. 10, together with REFRESCO results for five geometrically similar grids, showing the sensitivity of local spatial resolution. The elevation of the bow wave at the mast is shown in Fig. 11 for RANS $k - \omega$ SST, X-LES (Kok et al. 2004) and X-LES with adaptive mesh refinement (AMR) around the mast. The results show that the time averaged wave elevation is qualitatively comparable for all three cases: the overall flow features do not show considerable differences between the RANS prediction and the X-LES Scale-Resolving Simulations (SRS). On the

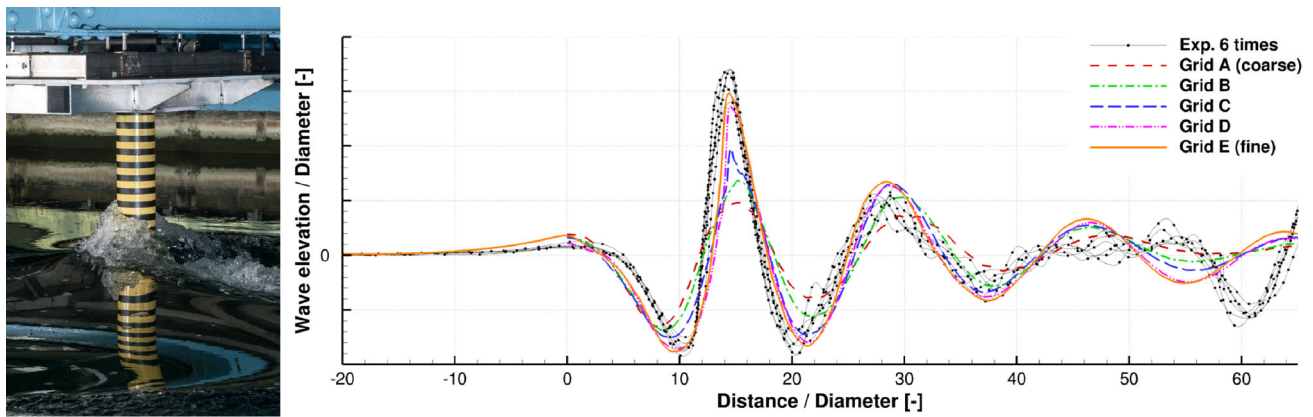


Fig. 10 Wave elevation (position relative to the cylinder, positive downstream) at lateral distance $5.64D$ from the centre of the cylinder, $Fr = 1.7$

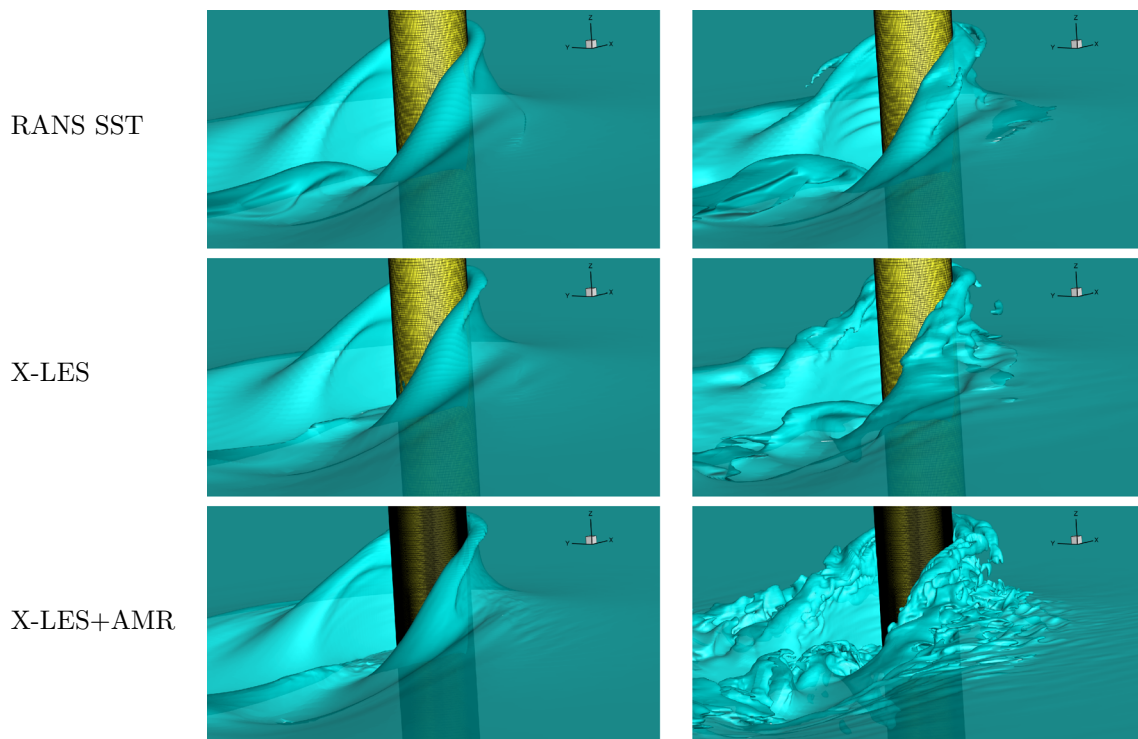


Fig. 11 Differences due to turbulence modelling and the use of adaptive mesh refinement (left: time averaged, right: instantaneous), $Fr = 1.7$

other hand, the instantaneous flow is very different between RANS and SRS, where the SRS shows much more dynamic behaviour of the breaking bow wave. Comparing this against the experiments as displayed in Fig. 12 gave a good visual match in terms of separation below the water surface and the breaking of the bow wave itself.

7 Depth keeping under waves

The ability to maintain depth when sailing at periscope depth is of paramount importance to submarines. Especially when operating in (irregular) waves, the vertical motion of the boat needs to be controlled. If the submarine rises too far,

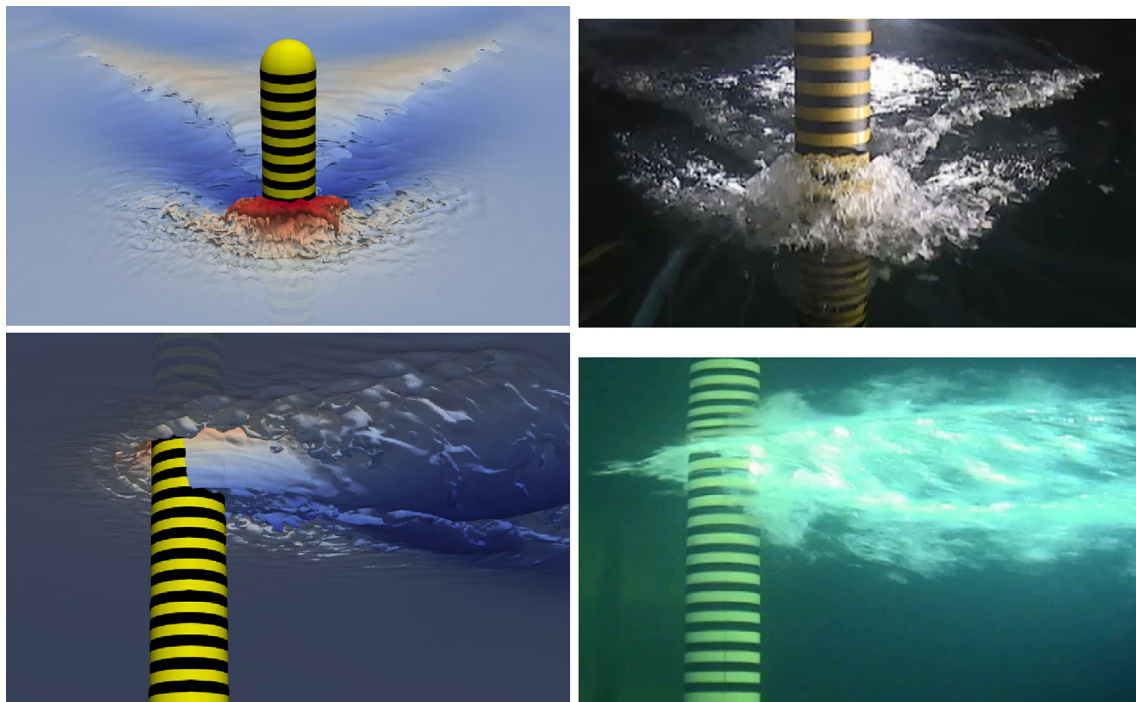


Fig. 12 Visual comparison of instantaneous CFD (left) and experimental (right) results, $Fr = 1.7$

the sail will emerge above the water surface which could lead to detection of the submarine. On the other hand, if the submarine sinks too far, periscopes and air intakes will submerge, possibly leading to loss of situational awareness and the forced shutting down of diesel engines. Hence, depth keeping at periscope depth is an important operational capability.

7.1 Effect of autopilot on depth keeping performance

The depth keeping performance of a submarine is strongly affected by the autopilot used to control the submarine. As the second-order wave forces introduce a constant disturbance, either a steady offset to the rudder angles or some type of integrating term in the autopilot is required to counteract this disturbance. The effect of this is seen in Fig. 13. The upper figure of Fig. 13 presents a time trace of the vertical position of a submarine, while the lower figure shows the time trace of the sail plane angle. The figure illustrates the response of the submarine and its sail plane angle during 1320 s in a bichromatic wave. The target depth is 12.75 m (indicated by the dashed line). Without an integrator in the autopilot, the submarine will sail on average at 13.5 m, while with integrator, the submarine sails on average at 12.75 m. The corresponding sailplane angle is on average 13.2° versus 12.5° . The difference in sail plane angle is small, but the average position difference of 0.75 m means the difference

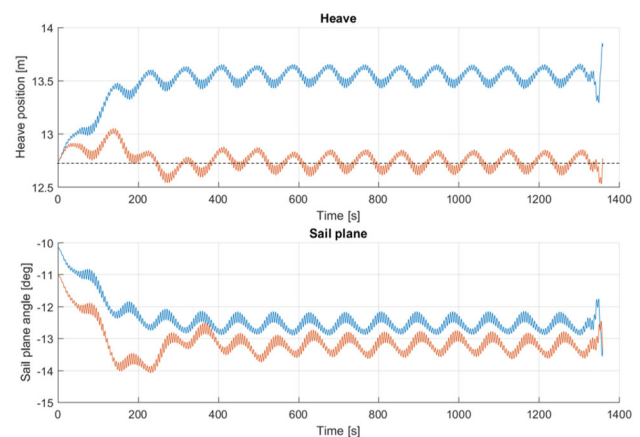


Fig. 13 Effect of adding an integrating term to a PID-heave autopilot. With the integrator (in orange), the heave stabilises around the starting value (indicated by the dashed line). Without the integrator (in blue) a steady offset remains

between periscope submergence or not. As a steady offset requires prior knowledge of the disturbance, which will be dependent on speed, sailing depth and wave direction, the use of an integrating term is preferred.

Changing the autopilot coefficients significantly effects the depth keeping performance. Unsuitable coefficients may lead to unstable behaviour. Optimising the coefficients stabilises the submarine's motions whilst minimising rudder usage. A fast time simulation model, such as SAMSON-XMF, is invaluable during the autopilot optimisation process.

It allows for efficient tuning, where the performance of various coefficients can be quickly compared to find the optimal performance.

7.2 Influence of waves on depth keeping performance

When sailing under waves, a submarine is subjected to wave forces which roughly can be decomposed into forces at the wave frequency and low frequent forces at the frequency of the wave groups. This is illustrated in Fig. 14. The upper figure of Fig. 14 shows a bichromatic wave train. The corresponding wave forces on the submarine are presented in the lower figure. Suppose that the submarine is keeping the same depth during this time series, then the wave frequent forces are directly related to the wave height. These wave frequent forces are an order of magnitude larger than the second-order wave drift forces shown in orange. The wave frequent forces oscillate between + 500 and – 500 kN, and the low frequent forces between 0 and 6 kN. Although the latter are considerably smaller than the first, the low frequent (or second order) forces have a non-zero mean value and tend to pull the submarine to the surface. It is important to take this second order force into account to accurately model the depth keeping performance of a submarine. The first order motions are of importance as they cause the heave motion, and obviously the wave elevation itself is of importance to know whether the periscope submerges or the sail emerges.

MARIN uses the time domain simulation program SAMSON-XMF [formerly SUBSIM or SAMSON (van Terwisga and Hooft 1988)] to simulate the manoeuvring and seakeeping of submerged submarines. A method has been devised to correctly model the important second order wave drift forces in the time domain simulations. This method is validated against various series of seakeeping model tests at periscope depth with multiple submarine geometries. An example of such a model test with the BB2 submarine is shown in Fig. 15.

To assess the depth keeping performance of a submarine, two aspects are of importance. Aspect one is that the depth keeping performance is dependent on the wave direction, sailing speed, selected autopilot and submerged depth of the submarine. This requires simulations or model tests for a large matrix of conditions. The second aspect is that long time traces are needed, because the nature of the vertical motion is not just based on wave frequent phenomena, but also on low frequent phenomena. To obtain insight in the actual depth keeping performance and reach statistical convergence, a long and sufficiently rich time trace is required.

A long time trace, as for instance shown at the top of Fig. 16, typically does not directly give insight in the performance. Although it is clear that the submarine has a certain range of vertical movement, it is nearly impossible to say

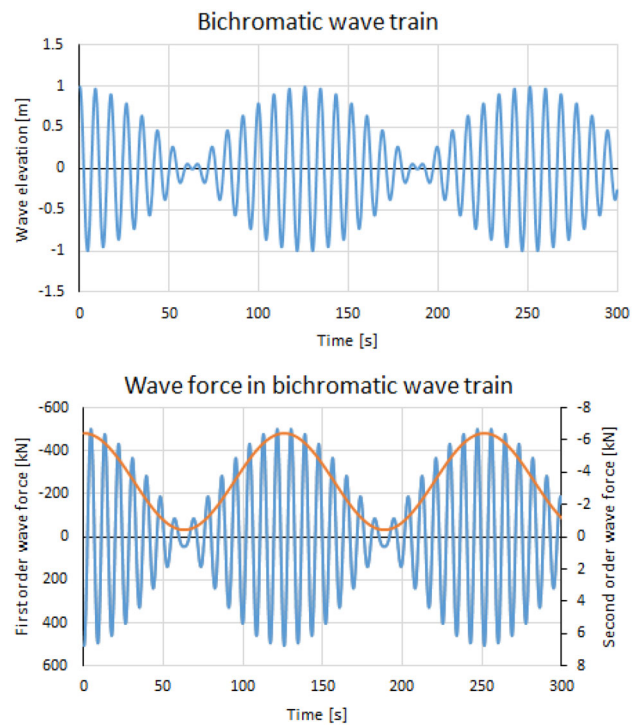


Fig. 14 The bichromatic wave shown in the top graph consists of two unidirectional waves of 0.70 and 0.75 rad/s. The bichromatic waves cause wave frequent forces (shown in blue in the lower graph) and low frequent forces (shown in orange). The low frequent forces have a non-zero mean value and oscillate at the frequency of the wave envelope

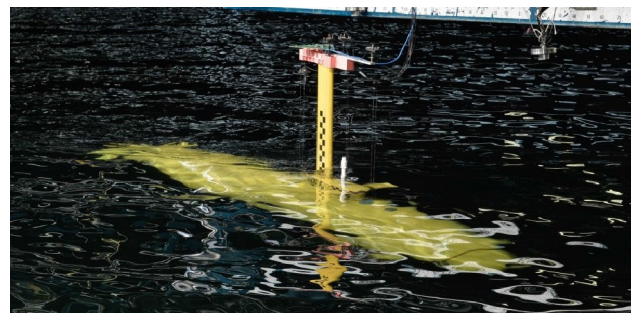


Fig. 15 Free running submerged model test with a submarine at periscope depth in irregular bow quartering waves in MARIN's Seakeeping and Manoeuvring Basin

from just the long time trace how often sail emergence or periscope submergence events occur.

To help assess the depth keeping performance, the long time traces at periscope depth are automatically processed to identify sail emergences and top-of-mast submergences. This is schematically shown for a part of the long time trace on the bottom left of Fig. 16. When the vertical position of the submarine is higher than the local wave elevation, the sail emerges (green) and when the submarine is too low with respect to the local wave elevation, the periscope is assumed to be submerged (red). The total number of sail emergence

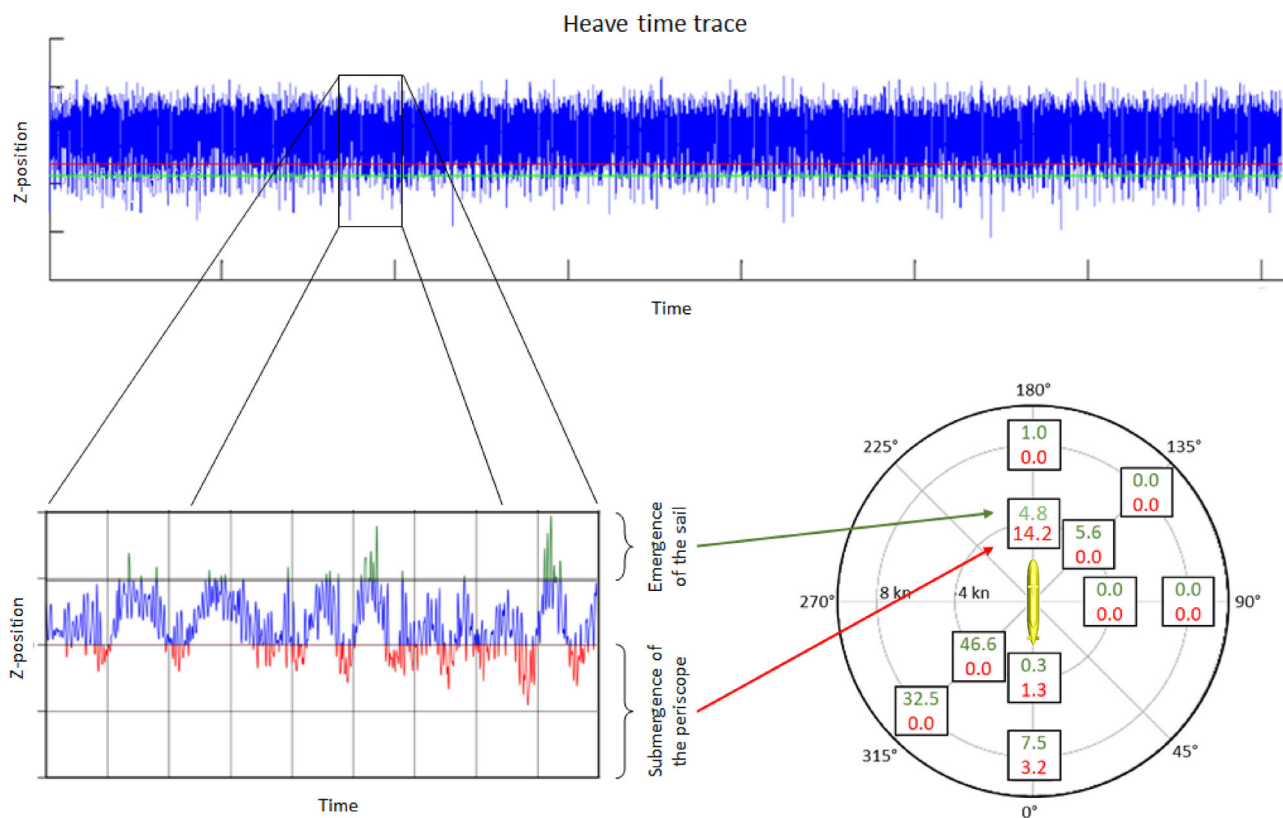


Fig. 16 An overview of the automatic data reduction used to determine the submarine's depth keeping performance. A long time trace of the submarine's vertical position (top) is analysed to identify cases of sail emergence (the parts of the time trace coloured green) and periscope submergence (the parts of the time trace coloured red). This analysis takes the local wave elevation into account. By combining the results

from various wave directions and sailing speeds in a single polar plot, the depth keeping performance can easily be compared to other submarine configurations. The polar plot on the bottom right shows the number of sail emergences (in green) and periscope submergences (in red) per half hour sailing time

and periscope submergence events are counted and the total and mean duration of the events over a given sailing period are determined. These derived quantities are reported as function of sailing speed, sea state and wave direction. Example results for the number of incidents over a given time period are shown on the bottom right of Fig. 16. Here, the radial position indicates the submarine's sailing speed (in knots), while the various wave directions are indicated by their angular position.

The data reduction thus achieved allows for a quantified and easy comparison of the depth keeping performance between various submarine and/or autopilot designs. Alternatively, operational limits of the submarine can be defined by comparing the depth keeping performance against operational criteria.

8 Conclusions

With the advance of experimental and numerical tools, the hydrodynamic design of submarines can be improved for the

complete operational profile of the boat. Off-design conditions can be taken into account when studying design options, such as improving the performance at the surface without significantly affecting the submerged characteristics of the boat. Especially the fast developments in CFD accuracy and performance but also advances in model testing techniques allow for detailed studies of the flow around submarines which leads to further understanding of the underlying hydrodynamics, and several examples are given in this article.

The length and bow studies indicate that hull shape modifications can improve surfaced performance while only having a limited impact on the submerged performance. A larger L/D ratio and a more slender bow will improve the overall powering performance across all operating conditions considerably. Near surface studies show the influence of the proximity of the free surface on the forces and moments acting on the submarine. In general, a suction force towards the free surface will be found when sailing at periscope depth, which is increased when also waves are present. The ability of an autopilot to maintain depth is largely influenced by these forces. To be able to avoid too much excursion from

the desired diving depth, second order wave forces need to be taken into account, as well as an integrating term in the autopilot controller.

When numerically studying submarine hydrodynamics, the appropriate tools need to be selected and they should be applied within their range of applicability. For example, when studying the performance of a submarine at periscope depth, potential flow codes will not be able to handle wave breaking which can occur when the sail is close to the water surface, or flow separation during manoeuvring conditions. For such applications, viscous flow solvers are more appropriate tools. Recent studies have shown the benefit of CFD for submarine hydrodynamics. In those studies, application of Automatic Mesh Refinement and Reynolds Stress Models to handle turbulence was found to be attractive to get good agreement with experiments.

With the current hydrodynamic tools, experience and knowledge, upkeep or successor programmes can be better supported than before.

Current CFD studies mainly focus on model scale conditions, due to the availability of validation material. However, some flow phenomena found on model scale are not as pronounced or different in full scale. For example, in full scale conditions, the flow will generally be turbulent and transition effects will have limited impact on the performance. On full scale, the boundary layer will also be thinner, and stall characteristics of control planes may be different. With a proper setup and with attention to controlling the numerical uncertainties in the results, CFD should be useful to study those effects as a function of Reynolds number. In future studies, more attention will therefore be paid to predictions for full-scale conditions.

Acknowledgements This research is partly funded by the Dutch Ministry of Economic Affairs and by the Dutch Defence Materiel Organisation under research programmes V1203, V1612 and M2004. The authors thank DSTG for kindly providing the BB2 wind tunnel measurement data set and QinetiQ for providing BB2 rotating arm experimental data.

Open Access This article is licensed under a Creative Commons Attribution 4.0 International License, which permits use, sharing, adaptation, distribution and reproduction in any medium or format, as long as you give appropriate credit to the original author(s) and the source, provide a link to the Creative Commons licence, and indicate if changes were made. The images or other third party material in this article are included in the article's Creative Commons licence, unless indicated otherwise in a credit line to the material. If material is not included in the article's Creative Commons licence and your intended use is not permitted by statutory regulation or exceeds the permitted use, you will need to obtain permission directly from the copyright holder. To view a copy of this licence, visit <http://creativecommons.org/licenses/by/4.0/>.

References

- Bettle MC, Toxopeus SL, Gerber AG (2010) Calculation of bottom clearance effects on Walrus submarine hydrodynamics. *Int Ship-build Prog* 57(3–4):101–125. <https://doi.org/10.3233/ISP-2010-0065>
- Carrica PM, Kerkvliet M, Quadvlieg FHHA et al (2016) CFD simulations and experiments of a maneuvering generic submarine and prognosis for simulation of near surface operation. In: 31st symposium on naval hydrodynamics, Monterey, CA
- Devenport WJ, Simpson RL, Dewitz MB et al (1992) Effects of a leading-edge fillet on the flow past an appendage-body junction. *AIAA J* 30(9):2177–2182. <https://doi.org/10.2514/3.11201>
- Eisfeld B, Brodersen O (2005) Advanced turbulence modelling and stress analysis for the DLR-F6 configuration. In: 23rd AIAA applied aerodynamics conference, Toronto, Canada, AIAA2005-4727. <https://doi.org/10.2514/6.2005-4727>
- Gertler M (1950) Resistance experiments on a systematic series of streamlined bodies of revolution—for application to the design of high-speed submarines. Tech. Rep. C-297, David W. Taylor Model Basin, Washington, DC
- Hay AD (1947) Flow about semi-submerged cylinders of finite length. Princeton University Report, Princeton, NJ
- Joubert PN (2006) Some aspects of submarine design—part 2. Shape of a submarine 2026. Tech. Rep. DSTO-TR-1920, Defence Science and Technology Organisation, Fishermans Bend, Victoria, Australia
- Kerkvliet M (2013) Influence on the numerical uncertainty of a generic submarine model by changing the wall-normal distribution of the wall-bounded grid cells. In: 16th numerical towing tank symposium (NuTTS). Müllheim, Germany, pp 78–83
- Klajj CM, Hoekstra M, Vaz G (2018) Design, analysis and verification of a volume-of-fluid model with interface-capturing scheme. *Comput Fluids* 170:324–340. <https://doi.org/10.1016/j.compfluid.2018.05.016>
- Klapwijk MD, Rotte G, Kerkvliet M et al (2017) Modelling of the plume of a submerged exhaust system. In: 20th numerical towing tank symposium (NuTTS), Wageningen, The Netherlands
- Kok JC, Dol HS, Oskam B et al (2004) Extra-Large Eddy Simulation of massively separated flows. In: 42nd AIAA aerospace sciences meeting and exhibit. American Institute of Aeronautics and Astronautics, Reno, Nevada, AIAA 2004-264. <https://doi.org/10.2514/6.2004-264>
- Lee SK, Manovski P, Kumar C (2018) Wake of a DST submarine model captured by stereoscopic Particle Image Velocimetry. In: 21st Australasian fluid mechanics conference, Adelaide, Australia
- NATO AVT-301 Task Group (2022) Flowfield prediction for manoeuvring underwater vehicles. NATO TR-AVT-301 Report
- Overpelt B (2014) Innovation in the hydrodynamic support for design of submarines. In: 12th international naval engineering conference and exhibition (INEC), Amsterdam, The Netherlands
- Overpelt B, Nienhuis B (2014) Bow shape design for increased surface performance of an SSK submarine. In: Warship 2014: naval submarines and UUV's, Bath, UK
- Overpelt B, Nienhuis B, Anderson B (2015) Free running manoeuvring model tests on a modern generic SSK class submarine (BB2). In: Pacific international maritime conference, Sydney, Australia
- Power JL (1977) Drag, flow transition, and laminar separation on nine bodies of revolution having different forebody shapes. Tech. Rep. 77-0065, David W. Taylor Naval Ship Research and Development Center, Bethesda, MD
- Raven HC (1996) A solution method for the nonlinear ship wave resistance problem. PhD thesis, Delft University of Technology
- Renilson MR (2018) Submarine hydrodynamics, 2nd edn. Springer, Cham. <https://doi.org/10.1007/978-3-319-79057-2>

- Torunski B (2018) Computational analysis of the free surface effects on a BB2 submarine undergoing horizontal maneuvers. Master's thesis, University of New Brunswick, Fredericton, New Brunswick, Canada
- Toxopeus SL (2008) Viscous-flow calculations for bare hull DARPA SUBOFF submarine at incidence. *Int Shipbuild Prog* 55(3):227–251. <https://doi.org/10.3233/ISP-2008-0048>
- Toxopeus SL, Atsavaprane P, Wolf E et al (2012) Collaborative CFD exercise for a submarine in a steady turn. In: 31st international conference on ocean, offshore and arctic engineering (OMAE), Rio de Janeiro, Brazil, OMAE2012-83573. <https://doi.org/10.1115/OMAE2012-83573>
- Toxopeus SL, Kuin R, Kerkvliet M et al (2014) Improvement of resistance and wake field of an underwater vehicle by optimising the fin-body junction flow with CFD. In: 33rd international conference on ocean, offshore and arctic engineering (OMAE), San Francisco, CA, OMAE2014-23784. <https://doi.org/10.1115/OMAE2014-23784>
- Toxopeus SL, Bettle MC, Uroić T et al (2019) NATO AVT-301 collaborative exercise: CFD predictions for BB2 generic submarine, phase 0—pre-test computations. In: NATO STO AVT-307 research symposium on separated flow: prediction, measurement and assessment for air and sea vehicles, Trondheim, Norway, STO-TR-AVT-307-22
- van Terwisga TJC, Hooft JP (1988) Hydrodynamic support in the design of submarines. In: Bicentennial maritime symposium. Australia, Sydney, pp 241–251
- Vaz G, Jaouen FAP, Hoekstra M (2009) Free-surface viscous flow computations. Validation of URANS code FRESKO. In: 28th international conference on ocean, offshore and arctic engineering (OMAE), Honolulu, Hawaii, OMAE2009-79398. <https://doi.org/10.1115/OMAE2009-79398>
- Vaz G, Toxopeus SL, Holmes S (2010) Calculation of manoeuvring forces on submarines using two viscous-flow solvers. In: 29th international conference on ocean, offshore and arctic engineering (OMAE), Shanghai, China, OMAE2010-20373. <https://doi.org/10.1115/OMAE2010-20373>

Publisher's Note Springer Nature remains neutral with regard to jurisdictional claims in published maps and institutional affiliations.